Available online at www.sciencedirect.com
ScienceDirect
Journal of Organometallic Chemistry 692 (2007) 2750–2760
Journal of Organometallic Chemistry
www.elsevier.com/locate/jorganchem

Structural control of dithiazolyl radicals: Case studies on 3′- and 4′-cyano-benzo-1,3,2-dithiazolyl, $NCC_6H_3S_2N$

Antonio Alberola, Jonathan Burley, Rebecca J. Collis, Robert J. Less, Jeremy M. Rawson *

Department of Chemistry, The University of Cambridge, Lensfield Road, Cambridge CB2 1EW, UK

Received 14 October 2006; received in revised form 6 December 2006; accepted 6 December 2006
Available online 23 December 2006

Abstract

Dithiazolyl radicals with π-stacking motifs have attracted particular interest because of their ability to exhibit spin-switching between diamagnetic distorted π-stacks and paramagnetic regular π-stacked structures through a solid state phase transition. Previous studies indicate that inclusion of electronegative heteroatoms into the backbone favours lamellar structures. This methodology has been extended to the synthesis and characterisation of the title compound, 4′-cyanobenzo-1,3,2-dithiazolyl (4-NCBDTA). Its electronic structure is probed through DFT calculations, cyclic voltammetry and EPR spectroscopy and its crystal structure determined by X-ray powder diffraction at room temperature. Variable temperature SQUID magnetometry reveals that 4-NCBDTA undergoes two phase transitions, each exhibiting bistability; a high temperature phase transition occurs at room temperature ($T_{C\downarrow} = 291$ K, $T_{C\uparrow} = 304$ K, $\Delta T = 13$ K); whilst the low temperature phase transition occurs below liquid nitrogen temperatures ($T_{C\downarrow} = 37$ K, $T_{C\uparrow} = 28$ K; $\Delta T = 9$ K).

Keywords: 1,3,2-dithiazolyl radicals

1. Introduction

There has been considerable interest in recent years in the development of molecular materials in which the bulk physical properties can be tailored at the molecular level [1]. Of considerable interest have been the physical properties associated with non-centrosymmetric structures such as piezo-, pyro- and ferro-electric materials as well as non-linear optic activity [2]. In other areas molecular materials have provided examples of electrically conducting [3] and magnetic materials [4]. In all these cases the physical properties are intimately associated with their solid state structure. As synthetic chemists, the manipulation of both the connectivity and electronic structure at the molecular level is usually within our capabilities, yet control of the weaker intermolecular forces (van der Waals, dipolar and electrostatic interactions) still offers a considerable challenge [5]. Whilst there has been some success in crystal structure prediction, [6] it is arguable that a large number of structures are rationalised in a 'post facto' manner. In this article we describe how we have utilised basic concepts in crystal engineering in order to construct new materials with well-defined physical properties. We shall also see that there are still a number of challenges which must be resolved if we are to proceed beyond a superficial approach to structure design.

Our work in this area stemmed from observations of bistability in the thiazyl radical TTTA (**1**) in which a solid-solid phase transition occurs between a diamagnetic 'low spin' distorted π-stack phase and a paramagnetic 'high spin' regular spaced π-stack [7]. This system is of particular interest since the temperatures for the low spin → high spin transition and high spin → low spin transitions are inequivalent. The consequence is a wide region of bistability for **1** in which both 'low spin' diamagnetic and 'high spin' paramagnetic phases are stable. For **1**, $T_{C(\downarrow)} = 230$ K and $T_{C(\uparrow)} = 320$ K providing a 90 K window of bistability

* Corresponding author. Tel.: +44 1223336319; fax: +44 1223336319.
E-mail address: jmr31@cus.cam.ac.uk (J.M. Rawson).

0022-328X/$ - see front matter © 2007 Elsevier B.V. All rights reserved.
doi:10.1016/j.jorganchem.2006.12.020

which encompasses room temperature. Work by Oakley has shown that other dithiazolyl radicals such as PDTA (**2**) and QDTA (**3**) exhibit similar behaviour [8]. Work by Awaga has shown that spin-switching in **1** can additionally be induced by light irradiation or application of pressure [9]. Structurally radicals **1**–**3** exhibit certain similarities, specifically the formation of π-stacked structures. Crystallographic studies indicate that the change in the magnetic response is associated with a structural distortion of the π-stack [7,8]. Our target has therefore been to develop new bistable materials through the systematic design of well-defined π-stacked structures. Particular objectives were (i) to prepare layer-like motifs; (ii) to investigate whether we are able to predict the nature of the intermolecular interactions within layers; (iii) establish whether there are further structural considerations which must be taken into account in order to develop new bistable switching materials.

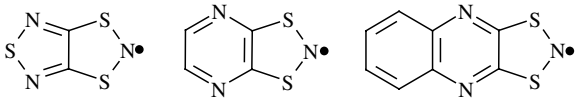

1 **2** **3**

2. Structures of aromatic π-systems

A number of studies on planar π-aromatics have indicated a strong tendency to adopt either of two basic structures; either a π-stack or a herringbone motif [10]. Detailed studies on benzene and related systems indicate that for aromatic hydrocarbons there are three types of intermolecular interactions; π···π, C–H···π and C–H···H–C. Of these the C–H···π interaction is *ca.* 12 kJ/mol whereas π–π interactions are *ca.* 8 kJ/mol [10]. As a consequence the majority of neutral aromatics adopt the more thermodynamically stable herringbone motif. This preference for herringbone motifs means that additional interactions must therefore be incorporated in order to stabilise π-stacked structures. These directional interactions embrace a large number of the so-called supramolecular synthons such as O–H···O, N–H···O as well as weaker C–H···O and C–H···N hydrogen-bonding motifs [10]. Hydrogen bonds are by no means exclusive and other structure-directing motifs have been identified such as CN···X (X = I, Br, Cl) [11]. In the case of thiazyl chemistry, S···N contacts are prevalent and S···N contacts between heterocyclic rings e.g. in thiadiazolyl rings [12] and CN···S interactions in dithiadiazolyl rings have been successfully used as structure-directing motifs [13].

3. A comparison of aromatic and N-substituted dithiazolyl radicals

The structures of benzodithiazolyl (BDTA) [14] and naphthyldithiazolyl (NDTA) [8] are presented in Fig. 1 and exhibit herringbone motifs typical of simple aromatics. Substitution of two C–H units by isoelectronic N atoms in the aromatic core of these two radicals chemically generates the isoelectronic pyrazine and quinoxaline derivatives (PDTA and QDTA). Both these radicals provide additional functionality for electrostatic interactions and both PDTA and QDTA radicals reported by Oakley adopt layer-like motifs in which the additional heterocyclic ring N atoms can be involved in electrostatically favourable interactions of the form C–H···N or S···N (Fig. 2) [8].

4. Development of new spin-transition dithiazolyl radicals

In order to prepare new dithiazolyl radicals capable of undergoing spin transitions analogous to TTTA and related π-stacked structures such as PDTA and QDTA we targeted the two novel radicals 3-NCBDTA and 4-NCBDTA in which the electronegative CN group was available for in-plane interactions to either the aromatic C–H or heterocyclic S atoms. A preliminary account of the synthesis and characterisation of 3-NCBDTA has recently been reported [15].

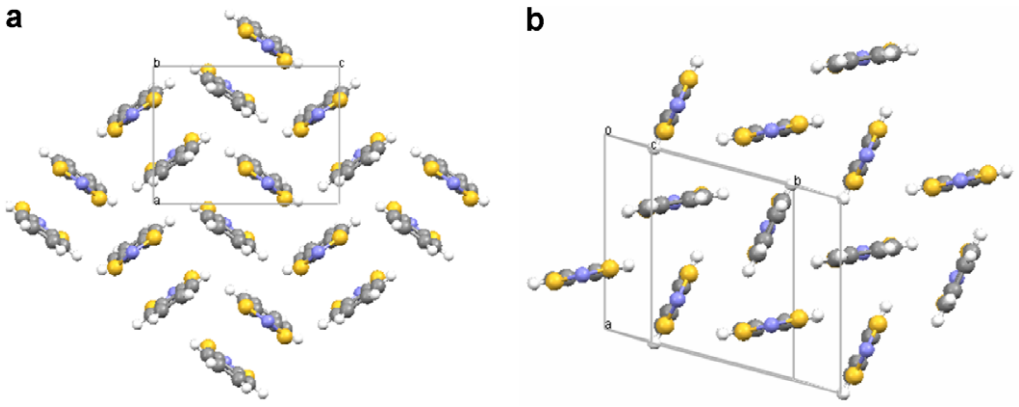

Fig. 1. Crystal structures of (a) BDTA and (b) NDTA.

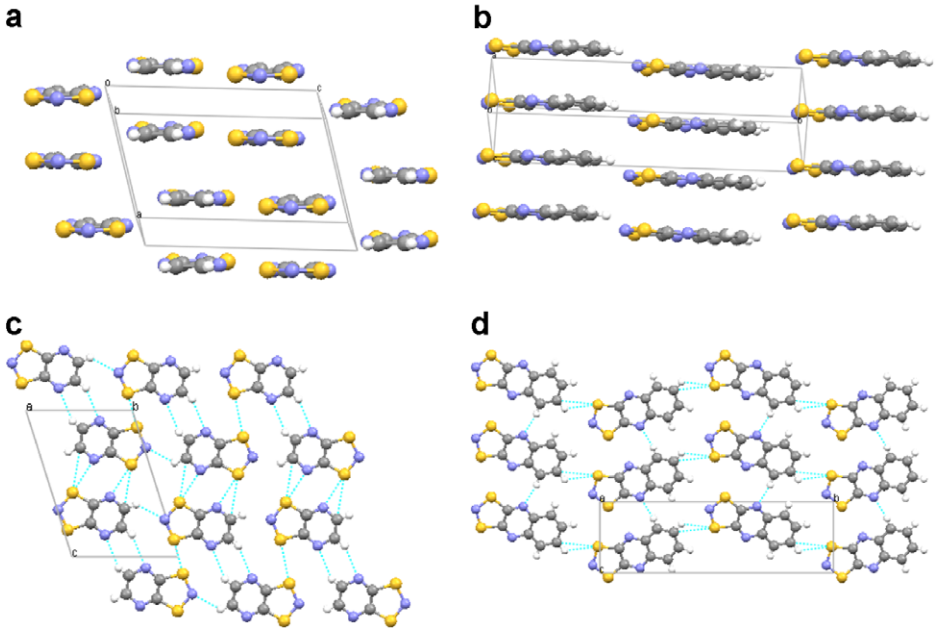

Fig. 2. Crystal structures of (a) PDTA and (b) QDTA viewed perpendicular to the stacking axis whilst (c) and (d) are views of PDTA and QDTA respectively parallel to the stacking axis.

4.1. Synthesis of 4-NCBDTA

The synthesis of 4-NCBDTA utilised the same methodology previously applied to the isomeric 3-NCBDTA [19]. In both cases the key benzo-substituted sulfenyl chloride was prepared in two steps from the parent dichlorobenzonitrile and "Less' reagent", [^{t}BuS]Na, which we have found provides a mild route into sulfenyl chloride chemistry; [15,16] Treatment of dichlorobenzonitrile with two equivalents of [^{t}BuS]Na in DMI (1,3-dimethyl-2-imidazolidinone) led to the dithiolate under mild conditions. The *tert*-butyl derivative is considerably bulky and deprotection of the thiolate occurs readily by chlorination with Cl_2 in CCl_4 at 0 °C. In comparison, reductive deprotection of thiolates to generate dithiols tends to require harsh conditions e.g. $Na/l \cdot NH_3$ which may not always support chemically sensitive functional groups [17].

Subsequent dissolution of the sulfenyl chloride in CH_2Cl_2 followed by condensation with Me_3SiN_3 generated the 4′-cyanobenzo-1,3,2-dithiazolylium chloride, [4-NCBDTA]Cl in good yield. This was then reduced with Ag powder in liquid SO_2 to generate the desired 4-NCBDTA which was subsequently purified by vacuum sublimation (10^{-1} Torr, 70–25 °C) (Scheme 1).

4.2. Electrochemical studies on 4-NCBDTA

Solutions of both 3-NCBDTA and 4-NCBDTA were studied by cyclic voltammetry and revealed reversible oxidation waves to the corresponding cations. These are presented in Fig. 3. The presence of the electron-withdrawing CN group leads to a stabilisation of the radical centre and a higher oxidation potential in relation to BDTA [+0.15 V vs SCE]; [13] 3-NCBDTA and 4-

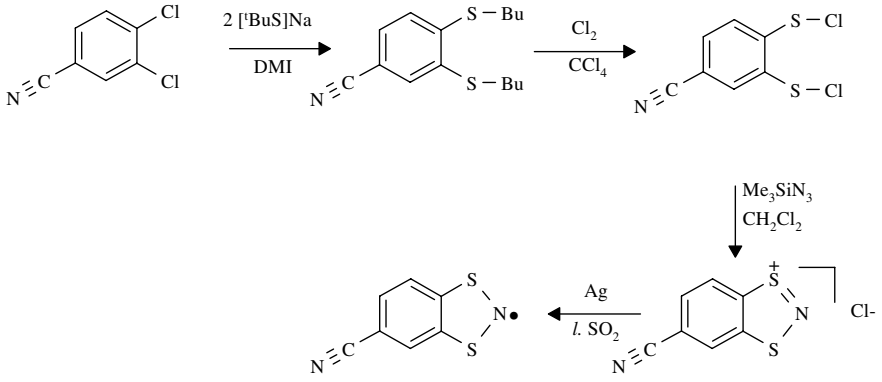

Scheme 1. Synthetic methodology for formation of 4-NCBDTA.

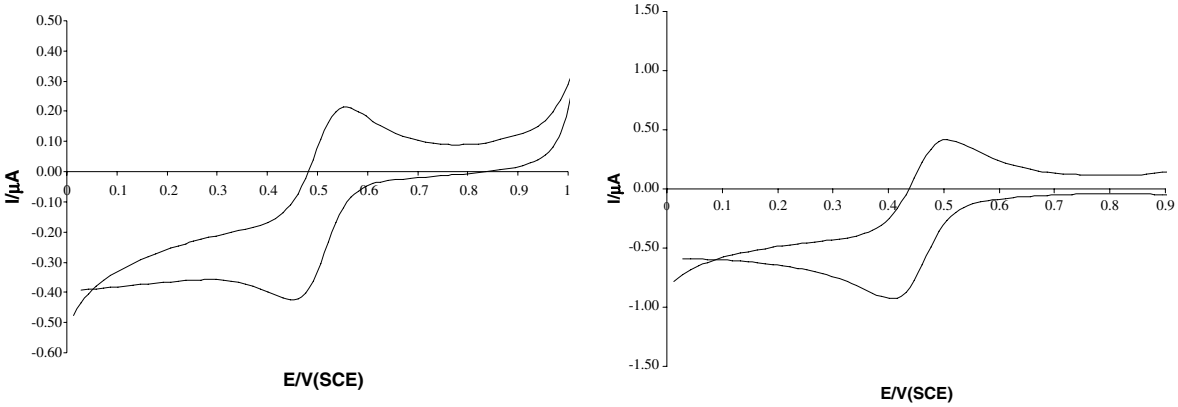

Fig. 3. Cyclic voltammograms of 3-NCBDTA (left) and 4-NCBDTA (right).

NCBDTA show reversible 1 e^- 0/+1 couples with $E_{1/2} =$ 0.491 V and 0.447 V respectively vs SCE.

4.3. EPR studies on 3-NCBDTA and 4-NCBDTA

EPR studies on frozen solutions of both compounds in THF were recorded at X-band and revealed a rhombic character typical of dithiazolyl radicals [18]. Both spectra revealed large hyperfine coupling to the dithiazolyl ring N but no hyperfine coupling to the nitrile N atom could be resolved indicating couplings similar to or less than the inherent linewidth of the EPR spectra (2.5 G). A typical spectrum is shown in Fig. 4. Both spectra could be simulated using similar sets of parameters (Table 1) indicating very small changes in spin density at the spin active ^{14}N nuclei.

4.4. Theoretical calculations on 3-NCBDTA and 4-NCBDTA

DFT calculations were performed on BDTA, 3-NCBDTA and 4-NCBDTA in order to probe the effect of cyano-substitution on the electronic structure and redox behaviour of these derivatives. The calculated spin density distributions are presented in Fig. 5.

The inclusion of the electron-withdrawing CN group leads to a small reduction in the calculated spin density at the SNS component of the dithiazolyl ring (91.1% of the calculated spin density residing on the S_2N fragment in BDTA *cf.* 85.8% and 88.1% in 3-NCBDTA and 4-NCBDTA respectively). Nevertheless the unpaired spin density at the dithiazolyl ring N atom is little affected at $46.3 \pm 1.0\%$ and the spin density at the cyano-N atom is small in both derivatives. As a consequence these small changes in spin density at the spin active ^{14}N nuclei are unlikely to be manifested in changes in EPR spectra. However the energy of the singly-occupied molecular orbital is lowered significantly for both cyano-derivatives indicating that they should be more readily generated by 1e^- reduction of the corresponding dithiazolylium cation. The invariance in EPR spectra and trends in electrochemical behaviour are in good agreement with these predictions.

The calculated molecular geometries for both cyano-substituted radicals are in reasonable agreement with those

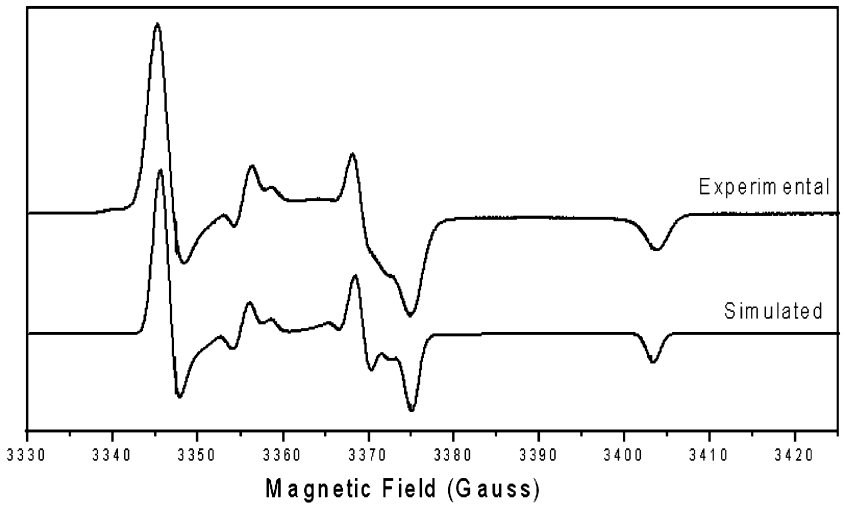

Fig. 4. Frozen solution EPR spectrum in dichloromethane at 220 K and simulation using parameters in Table 1 of 3-NCBDTA.

Table 1
Anisotropic EPR parameters used to simulate frozen solution spectra of 3-NCBDTA and 4-NCBDTA

g-Tensor	3-NCBDTA	4-NCBDTA	a_N	3-NCBDTA/G	4-NCBDTA/G
g_1	2.0130	2.0146	a_1^N	2.5	2.5
g_2	2.0051	2.0067	a_2^N	2.5	2.5
g_3	2.0017	2.0033	a_3^N	29.4	28.3
$\langle g \rangle$	2.0066	2.0082	$\langle a_N \rangle$	11.5	11.1

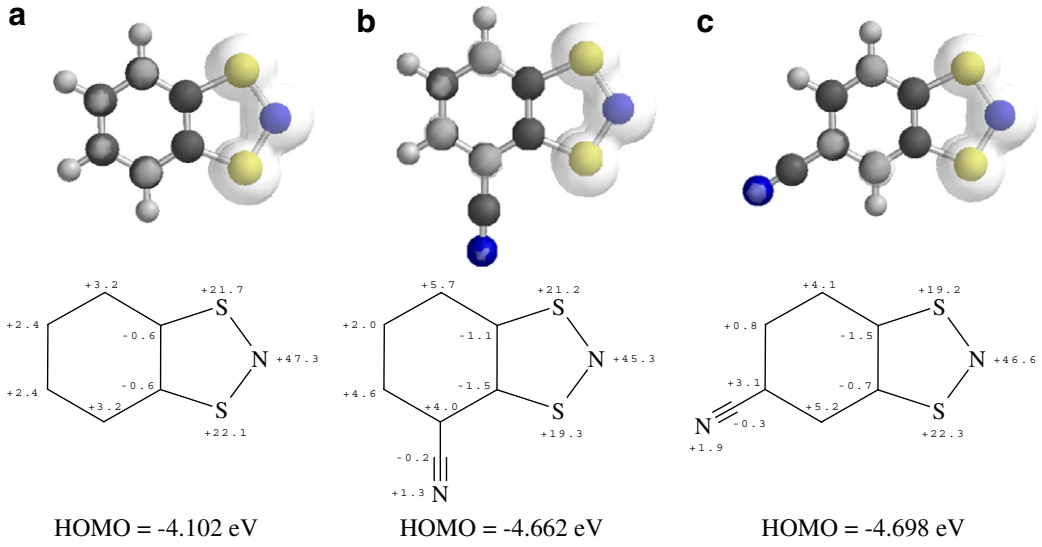

Fig. 5. Spin density distribution and HOMO energy calculated for: (a) BDTA; (b) 3-NCBDTA and (c) 4-NCBDTA.

determined by X-ray diffraction (Table 2) although the BP86/DN* basis set appears to slightly overestimate most bond lengths by ca. 1–2%.

4.5. Crystal structure of 3-NCBDTA

The crystal structures of 3-NCBDTA have been reported previously [15] but a brief description is included here for comparison to 4-NCBDTA and within the context of the discussion of the calculated molecular electrostatic isopotential maps (Section 4.7). At 180(2) K, 3-NCBDTA crystallises in the monoclinic space group $P2_1/c$ with two molecules in the asymmetric unit. These radicals form cofacial π^*–π^* dimers with intradimer S···S contacts of 3.263 and 3.347 Å.These adopt a distorted π-stacked motif along the crystallographic *a*-axis. The inter-dimer S···S contacts along this π-stacking direction are 3.886 and 3.971 Å. Within the *bc*-plane dimers are linked *via* alternating sets of S···N contacts between dithiazolyl rings ($d_{S\cdots N}$ = 3.149–3.287 Å) and CN···H–C contacts (2.645 Å) which propagate a ribbon-like motif parallel to the crystallographic *b*-axis (Fig. 6). The S···N contacts are similar to or a little less than the sum of the van der Waals radii of S and N (3.2 Å for in-plane contacts) [19]. The molecular planes of the two crystallographically independent molecules are inclined at 18.97° and 18.69° with respect to *bc*-plane. The twisting of the molecules out of the *bc*-plane affords an additional set of longer CN···H–C interactions between molecules in different layers ($d_{CN\cdots H}$ = 3.056 Å, Fig. 7a). These CN···H contacts are short and comparable with those seen in co-crystals of sym-tricyanobenzene [20a]. Indeed recent work [15] has suggested that the cyano-nitrogen atom is better able to act as a hydrogen bond acceptor than more conventional acceptors such as amines and thus short contacts to weak H-bond donors such as aromatic C–H groups are probably significant.

At 300 K the unit cell of 3-NCBDTA is halved. Whilst it retains the monoclinic $P2_1/c$ setting there is now a single molecule in the asymmetric unit and a regular spacing (3.665 Å) of radicals parallel to the crystallographic *a*-axis. Within the *bc*-plane the radicals retain both the S···N and CN···H–C contacts identified in the low temperature phase. The S···N contacts are now located about an inversion centre but slightly longer than in the low temperature structure with S···N = 3.322 Å. The corresponding in-plane CN···H–C contacts are also located about an inversion centre. The CN···H contacts (2.818 Å) now lie midway between the intra-plane and inter-plane contacts observed in the low temperature phase.

4.6. Crystal structure of 4-NCBDTA

Attempts to grow suitable crystals of 4-NCBDTA for single-crystal X-ray diffraction at a range of temperatures above and below the high temperature phase transition region (identified from SQUID data to be between 291

Table 2
Heterocyclic bond lengths and angles for 3-NCBDTA and 4-NCBDTA with those determined by DFT theory

	3-NCBDTA		4-NCBDTA	
	Observed[a]	Calculated	Observed	Calculated
Bond length (Å)				
C–C	1.394(8)[b] 1.399(4) 1.397(4)	1.417	1.394(7) 1.394(9)	1.419
C–S	1.742(6)[b] 1.746(3) 1.749(3)	1.760	1.742(8) 1.742(6)	1.751
S–N	1.634(6)[b] 1.642(3) 1.650(2)	1.667	1.633(7) 1.632(7)	1.668
N–S	1.673(6)[b] 1.655(3) 1.650(3)	1.665	1.673(6) 1.673(6)	1.671
S–C	1.737(5)[b] 1.743(3) 1.742(3)	1.753	1.738(9) 1.738(8)	1.763
Bond angle (°)				
C–S–N	100.0(3)[b] 100.45(13) 99.82(13)	99.78	100.01(11) 100.02(12)	100.03
S–N–S	114.5(3)[b] 114.29(14) 114.48(14)	114.26	114.59(15) 114.62(14)	114.09
N–S–C	98.4(3)[b] 98.95(13) 99.16(13)	99.64	98.39(13) 98.35(14)	99.52
S–C–C	114.4(4)[b] 114.4(2) 114.1(2)	113.57	114.37(14) 114.40(15)	113.18
C–C–S	112.6(5)[b] 111.8(2) 112.4(2)	112.75	112.6(3) 112.6(5)	113.17

[a] Number marked.
[b] Corresponds to the high temperature phase.

and 304 K) have so far proved fruitless. However sublimed samples provided good quality X-ray powder diffraction patterns over the temperature range 250–350 K. Besides

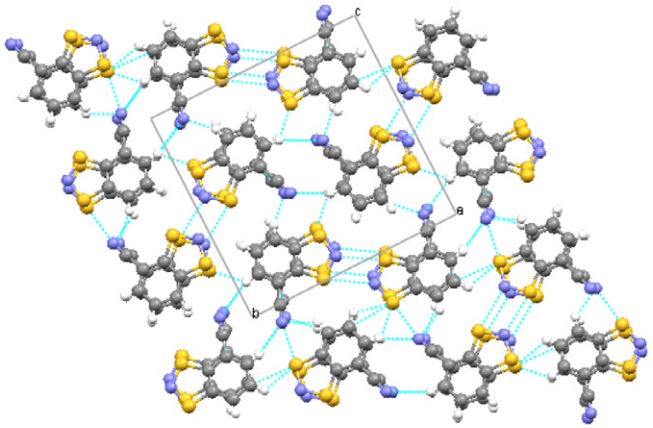

Fig. 6. Structure of 3-NCBDTA at 180(2) K viewed parallel to the *a*-axis.

the normal effects due to thermal expansion there is no clear evidence from the diffraction data of any phase transition on warming from 250 to 350 K. The absence of super-lattice reflections below 290 K (expected for a Peierls distortion of the one-dimensional π-stack) may reflect diffuse/weaker scattering from the super-lattice reflections.

Structure solution from powder diffraction data has developed rapidly over the last 10 years [21] and has been applied to a range of both organic and inorganic materials, although it is still far from being a routine technique. Nevertheless we have been successful in applying this methodology to a number of thiazyl radicals [22] and it proved possible to solve the structure of **3** from X-ray powder diffraction data. Full details of the structure solution of **3** are presented in the Supporting Information.

The powder pattern at 330 K was indexed on a monoclinic cell ($P2_1$) whose volume indicated two crystallographically independent molecules in the asymmetric unit. Structure solution and refinement revealed a structure with striking similarities to 3-NCBDTA. Specifically the molecules adopt a layer-like structure within the *ab*-plane. Close contacts comprise a set of CN···H–C interactions with similar geometric parameters ($d_{CN\cdots H} = 2.554$ Å) to 3-NCBDTA albeit with shorter C–N···H contacts. However, whilst in-plane S···N contacts are retained, the centrosymmetric S···N motif in 3–NCBDTA is replaced by

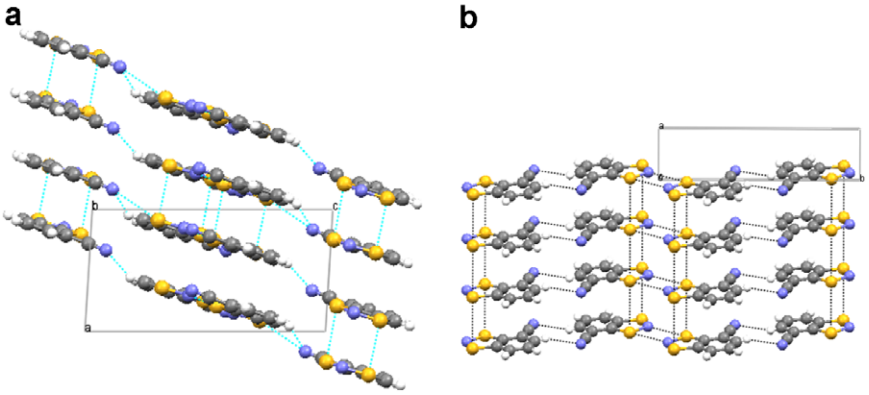

Fig. 7. Structure of 3-NCBDTA viewed (a) in the *ac*-plane at 180(2) K and (b) in the *ab*-plane at 300(2) K.

a near linear N–S···N–S contact which generates a chain parallel to the crystallographic *b*-axis ($d_{S\cdots N} = 2.880$ and 3.062 Å, *cf.* sum of the van der Waals radii for S and N at 3.20 Å) [19]. The result is a set of two crystallographically independent but co-parallel chains parallel to the crystallographic *b*-axis with each chain comprising S···N contacts. Independent chains are then linked *via* CN···H–C contacts (Fig. 8). Like 3-NCBDTA molecules are twisted with respect to these layers. In 4-NCBDTA one is inclined at 7.34° whereas the second independent molecule is inclined at 21.81°.

Perpendicular to the stacking axis radicals form a regular π-stack with S···S separations of 3.619 Å (equivalent to the crystallographic *c*-axis) and comparable to that observed for the high temperature phase of 3-NCBDTA (3.665 Å at 300(2) K). The twisting of the molecules out of the molecular plane facilitates additional short interplane CN···H–C contacts ($d_{CN\cdots H-C} = 2.588$ Å) of similar geometry to the in-plane contacts. These contacts generate a helical arrangement along the crystallographic *c*-axis (Fig. 9).

4.7. Analysis of the structures of 3-NCBDTA and 4-NCBDTA

The MEPs of these two radicals are illustrated in Fig. 10. In both cases the cyano group bears the largest partial negative charge with smaller contributions on the heterocyclic dithiazolyl ring N atom. In both cases the molecular structures would appear to favour either of the electrostatically favourable CN···S or CN···H–C interactions and a CN···H–C interaction appears as a recurrent theme. Notably in both PDTA and QDTA the corresponding pyridyl-N···H–C interactions appeared structure-directing. Whilst the CN···H–C motif persists in both 3-NCBDTA and 4-NCBDTA, the centrosymmetric S···N dimer motif (common to thiazyl systems) [12] is present

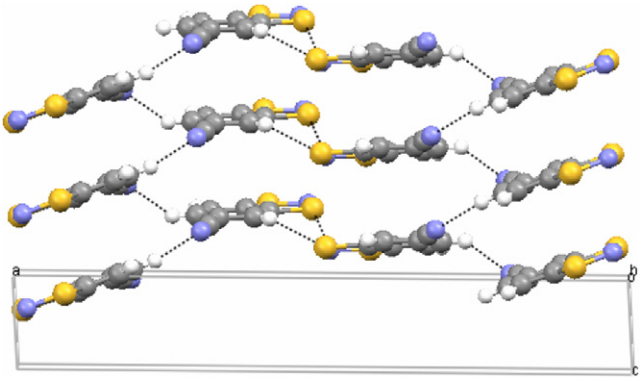

Fig. 9. View of 4-NCBDTA illustrating the interlayer CN···H–C contacts.

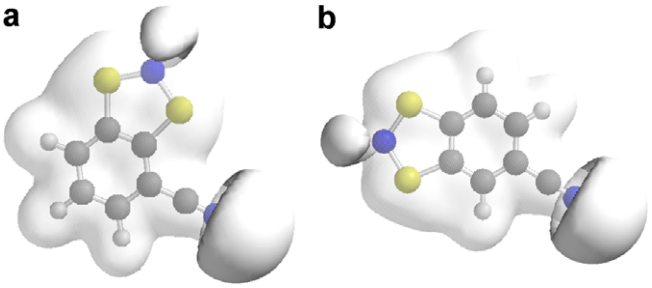

Fig. 10. Molecular electrostatic isopotential surfaces for (a) 3-NCBDTA and (b) 4-NCBDTA.

in 3-NCBDTA but absent in 4-NCBDTA. This would suggest that the CN···H–C contact is more favourable.

In 3-NCBDTA each molecule offers one CN and one C–H group for this interaction and the shortest of the intermolecular CN···H interactions generate dimers close to the *bc*-plane. In 4-NCBDTA each molecule again offers one CN group and a C–H hydrogen bond donor. However

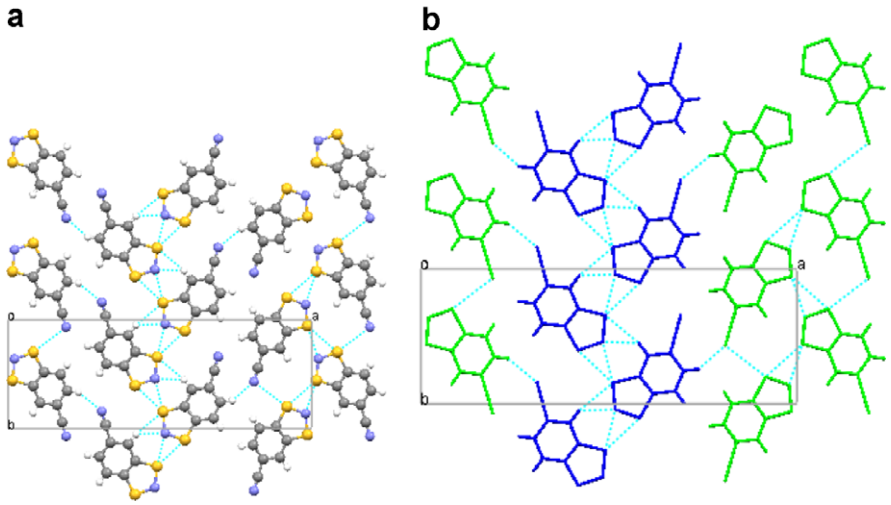

Fig. 8. View of (a) 4-NCBDTA in the *ab*-plane and (b) crystallographically independent molecules emphasize the two sets of independent S···N chains linked via the CN···H–C contacts.

the molecules of 4-NCBDTA are twisted out of the *ac*-plane so as to form layers linked *via* CN···H contacts (Fig. 9). We believe that these different methods of propagation of the CN···H contacts lie at the origin of the subtle differences in their magnetic properties (section 5.10).

4.8. Magnetic studies on 3-NCBDTA and 4-NCBDTA

The magnetic properties of π-stacked DTA radicals are typically reflected in a diamagnetic-paramagnetic phase transition which is associated with a solid-state transformation from regular π-stack to distorted π-stack motif [23]. With the exception of 3-NCBDTA (which we reported recently [19]) the phase transition is typically associated with a region of bistability i.e. there is a temperature regime in which both diamagnetic and paramagnetic phases can co-exist and in which the magnetic response is strongly dependent upon sample history [7,8]. In some instances the temperature region of bistability can be large (>90 K).

Magnetic susceptibility measurements on 4-NCBDTA were made on a Quantum Design SQUID magnetometer in an applied field of 5000 G between 5 K and 350 K. Data were corrected for both sample diamagnetism (Pascal's constants) and the sample holder.

On heating a sample of 4-NCBDTA from 270 to 350 K an abrupt phase transition is observed at 304 K (31 °C) to a paramagnetic state. The value of χT then increases steadily up to 350 K, reaching a value of 0.04 emu.K.Oe^{-1}mol^{-1}, just 10% of that expected for an $S = 1/2$ paramagnet. This is consistent with a very strongly correlated electronic regime and comparable to the value of 0.16 emu.K.Oe^{-1}mol^{-1} at 350 K for **1** [7]. This phase transition was found to be reversible (Fig. 11a) but, unlike 3-NCBDTA, it does exhibit thermal hysteresis ($T_{C\downarrow} =$ 291 K, $T_{C\uparrow} = 304$ K, $\Delta T = 13$ K).

Upon cooling the sample of 4-NCBDTA undergoes a second magnetic phase transition from a diamagnetic phase to a second paramagnetic phase. The discontinuity in χ associated with this transition mitigates against contamination with an $S = 1/2$ Curie spin [24]. This transition also exhibits thermal hysteresis ($T_{C\downarrow} = 37$ K, $T_{C\uparrow} = 28$ K; $\Delta T = 9$ K) (Fig. 11b) and is comparable to the low temperature phase transition observed in 3-NCBDTA ($T_{C\downarrow} = 40$ K, $T_{C\uparrow} = 25$ K; $\Delta T = 15$ K). Previous studies on spin-transition compounds [7,8,25] typically favour the entropically stabilised paramagnetic regime at higher temperature. The phase transition to a paramagnetic phase upon cooling is therefore highly unusual. Moreover the thermal hysteresis in this low temperature regime is also anomalous; the phase transition temperature for both 3-NCBDTA and 4-NCBDTA upon warming occurs ***below*** the phase transition for the cooling process. This should be contrasted with other bistable materials in which the phase transition on warming typically occurs above the phase transition for the cooling process, as is the case for the high temperature phase transition in 4-NCBDTA (Section 4.9).

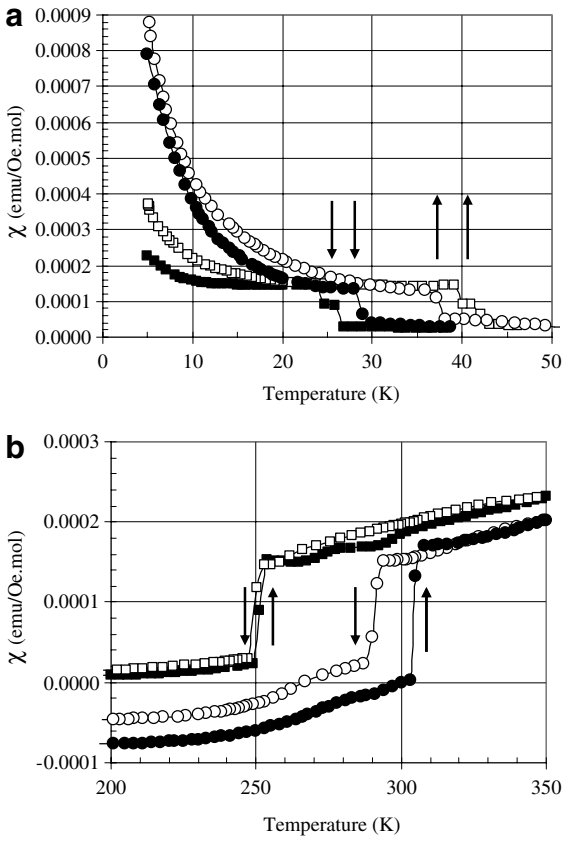

Fig. 11. Temperature dependence of χ for both 3-NCBDTA upon heating (●) and cooling (○) and 4-NCBDTA upon heating (■) and cooling (□) in (a) the low temperature regime (<50 K) and (b) the high temperature regime (200–350 K).

4.9. Mechanism of phase-switching

The further development of spin-switching materials based on dithiazolyl radicals relies heavily on developing an understanding of the mechanism of the phase transition and the origins of the bistability. The origin of the thermal hysteresis has been associated with a large activation barrier to structural reorganisation from an enthalpically stabilised distorted π-stack and an entropically stabilised regular stack. Previous work by Oakley has focused on the cleavage and reformation of inter-layer S···N contacts between molecules as the likely origin of this activation energy in TTTA and PDTA [8]. The inter-layer contacts arise through tilting of the molecule with respect to the stacking axis in the regular stacked phases and formation of in-plane contacts in the low temperature distorted π-stack structures.

In the case of 3-NCBDTA there is no hysteresis ($\Delta T < 1$ K) associated with the phase transition indicative of a minimal reorganisation energy. Indeed the electrostatically favourable intermolecular S···N and CN···H contacts in 3-NCBDTA lie within the layers with the two independent molecules twisted by just 3.7° from coplanarity in the low temperature phase and coplanar in the high temperature phase. The corresponding S···N and CN···H

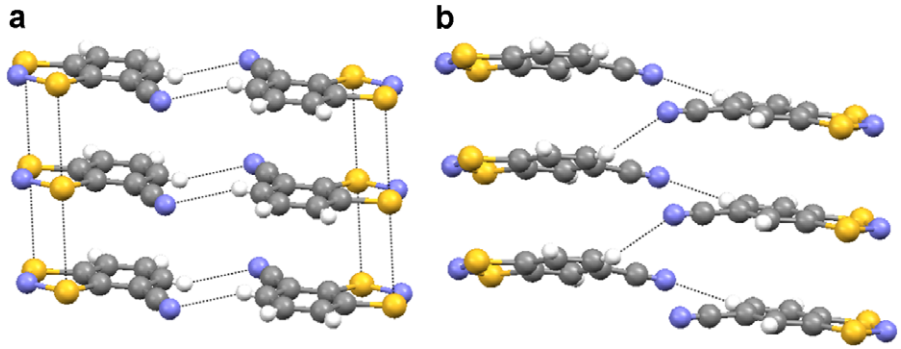

Fig. 12. Propagation of electrostatically favourable CN···H–C motifs generating (a) discrete centrosymmetric dimers in 3-NCBDTA and (b) chains in 4-NCBDTA.

interstack contacts between layers are substantially longer. Consequently the structural reorganisation via a distortion along the *a*-axis can occur without cleavage of the strong inter-stack contacts.

In the case of 4-NCBDTA only the structure of the high temperature phase is unambiguously identified. Here there are two crystallographically independent molecules. Whilst one molecule lies close to the *ab*-plane (7.34°), the second is twisted more substantially out of this plane (21.81°). This gives rise to a set of S···N contacts close to the molecular plane ($d_{S\cdots N} = 3.062$ Å) and between different planes ($d_{S\cdots N} = 3.355$ Å). In addition the twisting also facilitates CN···H contacts in which the CN···H contacts between molecules in neighbouring layers are near equivalent $d_{CN\cdots H} = 2.554$ and 2.588 Å and also shorter than those in 3-NCBDTA. A comparison of the CN···H contacts in 3-NCBDTA and 4-NCBDTA are presented in Fig. 12. Whilst 3-NCBDTA can undergo a lattice distortion without cleavage of intermolecular CN···H contacts, dimerisation in 4-NCBDTA is likely to proceed *via* cleavage and reformation of the interstack CN···H contacts.

At the present time there is no structural information on the low temperature phase transitions observed for both materials. However the similarities in both the positions of their phase transitions and their solid-state motifs would indicate that the low temperature processes in both cases are likely to be similar. Indeed the limited thermal energy available would indicate that this structural rearrangement must follow a low energy pathway which disrupts the π^*–π^* dimerisation motif. A glide between layers is plausible but further low temperature studies are required.

5. Conclusions

An analysis of the structures of simple neutral aromatic molecules proves to be instructive in the design of dithiazolyl radicals, leading to a controlled predilection for either π-stacked or herringbone motifs. This work has been extended to the synthesis of two cyano-functionalised benzodithiazolyl radicals which exhibit layer-like motifs. The importance of the CN···H contact is identified in the calculated molecular electrostatic isopotential maps and reflected in the observed π-stacked structures.

Both 3-NCBDTA and 4-NCBDTA exhibit phase transitions between regular and distorted π-stacked motifs. In 3-NCBDTA this occurs without thermal hysteresis at 250 K whereas in 4-NCBDTA a small region of thermal hysteresis is observed ($T_{C\downarrow} = 291$ K, $T_{C\uparrow} = 304$ K, $\Delta T = 13$ K). The absence of bistability in 3-NCBDTA and presence in 4-NCBDTA has been attributed to the activation energy associated with the cleavage of interlayer S···N and particularly CN···H contacts during the solid state transformation. Whilst layer-like structures favour spin-switching, the evidence here suggests that rotation of the molecular plane with respect to the normal to the stacking direction facilitates interstack/interlayer contacts which appears important for bistability.

In addition to these high-temperature phase transitions, both 3-NCBDTA and 4-NCBDTA exhibit low-temperature transitions with thermal hysteresis. In both cases the behaviour is unprecedented, with the spin transition driven to the paramagnetic phase upon cooling. In addition the phase transition exhibits an unusual 'inverse' behaviour of the hysteresis, the origins of which are under further investigation.

Further studies are underway to probe the low temperature phase transitions in both 3-NCBDTA and 4-NCBDTA, as well as prepare further bistable materials in which the molecular orientations are tailored to modify the window of bistability.

6. Experimental

6.1. Synthesis of 3-NCBDTA

2,3-Dichlorobenzonitrile (2 g, 11.6 mmol) was dissolved in 1,3-dimethyl-2-imidazolidinone (20 ml). Sodium butyl thiolate (4.7 g, 43 mmol) was added and the reaction mixture heated to 60 °C for 24 h. After allowing the reaction mixture to cool to room temperature, water (100 ml) was added and the mixture extracted with diethyl ether (3 × 75 ml). The organic extracts were combined and washed with water and brine, and the solvent removed *in vacuo*. The product was recrystallised from diethylether to afford pure $C_6H_3(CN)(S^tBu)_2$ (1.9 g, 57%). Analysis found: C 67.43; H 7.58; N 5.04; $C_{15}H_{21}S_2N$ requires: C

64.47; H 7.57; N 5.01%. δH ($CDCl_3$) 1.32 (s, 18H), 7.41 (t, 1H), 7.70 (dd, 1H), 7.95 (dd, 1H). m/z (EI) 279.1 (M^+, 100%).

Chlorination of $C_6H_3(CN)(S^tBu)_2$ (1.0 g, 3.5 mmol) in CCl_4 (20 ml) under ambient conditions yielded an orange solution of $C_6H_3(CN)(SCl)_2$. The solvent was removed *in vacuo* and the oily residue redissolved in CH_2Cl_2 (20 ml). This was treated with Me_3SiN_3 (0.4 ml, 5 mmol) to yield the salt [3-NCBDTA][Cl]. Reduction with Ag powder in *l.* SO_2 (20 ml) yielded 3-NCBDTA (0.236 g, 35%) which was purified by vacuum sublimation. Analysis found: C 49.46; H 1.73; N 15.24; $C_7H_3S_2N_2$ requires: C 49.9; H 1.68; N 15.63%.

6.2. Synthesis of 4-NCBDTA

3,4-Dichlorobenzonitrile (2 g, 11.6 mmol) was dissolved in 1,3-dimethyl-2-imidazolidinone (20 ml). Sodium butyl thiolate (4.7 g, 43 mmol) was added and the mixture heated to 60°C for 24 h. After cooling room temperature, water (100 ml) was added and the mixture extracted with diethyl ether (3 × 75 ml). The organic extracts were combined and washed with water and brine, and the solvent removed *in vacuo*. The product was recrystallised from diethylether to afford pure $C_6H_3(CN)(S^tBu)_2$ (2 g, 61%). Analysis found: C 64.81; H 7.63; N 4.98. $C_{15}H_{21}S_2N$ requires: C 64.47; H 7.57; N 5.01%. δH ($CDCl_3$) 1.41 (s,18H), 7.47 (dd, 1H), 7.68 (d,1H), 7.85 (d, 1H). *m/z* (EI) 279.1 (M^+, 100%).

Chlorination of $C_6H_3(CN)(S^tBu)_2$ (1.0 g, 3.5 mmol) in CCl_4 (20 ml) under ambient conditions yielded an orange solution of $C_6H_3(CN)(SCl)_2$. The solvent was removed *in vacuo* and the oily residue redissolved in CH_2Cl_2 (20 ml). This was treated with Me_3SiN_3 (0.4 ml, 5 mmol) to yield the salt [4-NCBDTA][Cl]. The salt was reduced with Ag powder in *l.* SO_2 (20 ml) to yield 4-NCBDTA (0.314 g, 46%) which was purified by vacuum sublimation. Analysis found: C 46.91; H 1.70; N 15.62. $C_7H_3S_2N_2$ requires: C 49.91; H 1.68; N 15.63%.

6.3. Theoretical calculations

6.3.1. Experimental

Preliminary UHF DFT calculations (LSDA/pBP86/DN*) were carried out within Spartan Pro [26]. This approach utilises a perturbative Becke-Perdew (pBP86) procedure [27] within the local spin density approximation LSDA. Instead of Gaussian basis sets, Spartan Pro utilises atomic solutions supplemented with d-type functions for heavy atoms, including numerical polarisation (DN*). It is generally considered that the pBP86 method compares most closely to the Gaussian B88-P86 method, whilst the DN* basis set is close to 6-311+G*. Comparisons of DFT methods can be found in articles cited in Ref. [28]. Initial trial geometries were determined using semi-empirical methods (PM3) and then optimised freely. All structures were stationary points with no imaginary frequencies consistent with energy minima.

Acknowledgements

We would like to thank the EPSRC for financial support (R.J.L. and R.J.C.); Homerton College and Jesus College Cambridge for Fellowships (A.A. and J.B. respectively); Prof. Coronado at the University of Valencia for use of the SQUID magnetometer and; Prof. Sanders (University of Cambridge) for access to the PC Spartan Pro software for preliminary DFT calculations.

References

[1] A.M. Reed, J.M. Tour, Sci. Am. 86 (2002) 282;
M.D. Ward, Chem. Soc. Rev. 24 (1995) 121.
[2] Ch. Bosshard, K. Sutter, Ph. Pretre, J. Hulliger, M. Florsheimer, P. Kaatz, P. Gunter, Organic Nonlinear Optical Materials, Gordon and Breach, Basel, 1995.
[3] B.E. Bowler, A.L. Raphael, H.B. Gray, Prog. Inorg. Chem. 38 (1990) 259.
[4] J.S. Miller, A.J. Epstein, Angew. Chem. Int. Ed. Engl. (1994) 385.
[5] M.D. Hollingsworth, Science (2002) 2410.
[6] See for example: J.P.M. Lommerse, W.D.S. Motherwell, H.L. Ammon, J.D. Dunitz, A. Gavezzotti, D.W.M. Hofmann, F.J.J. Leusen, W.T.M. Mooij, S.L. Price, B. Schweizer, M.U. Schmidt, B.P. van Eijck, P. Verwer, D.E. Williams, Acta Crystallogr. B 56 (2000) 697.
[7] W. Fujita, K. Awaga, Science (1999) 281;
G.D. McManus, J.M. Rawson, N. Feeder, J. van Duijn, E.J.L. McInnes, J.J. Novoa, R. Burriel, F. Palacio, P. Oliete, J. Mater. Chem. 11 (2001) 1992.
[8] J.L. Brusso, O.P. Clements, R.C. Haddon, M.E. Itkis, A.A. Leitch, R.T. Oakley, R.W. Reed, J.F. Richardson, J. Am. Chem. Soc. 126 (2004) 14692;
J.L. Brusso, O.P. Clements, R.C. Haddon, M.E. Itkis, A.A. Leitch, R.T. Oakley, R.W. Reed, J.F. Richardson, J. Am. Chem. Soc. 126 (2004) 8256;
T.M. Barclay, A.W. Cordes, N.A. George, R.C. Haddon, R.T. Oakley, T.T.M. Palstra, G.W. Patenaude, R.W. Reed, J.F. Richardson, H. Zhang, J. Chem. Soc., Chem. Commun. (1997) 873.
[9] H. Matsuzaki, W. Fujita, K. Awaga, H. Okamoto, Phys. Rev. Lett. 91 (2003) 017403;
W. Fujita, K. Awaga, Chem. Phys. Lett. 393 (2004) 150.
[10] G.R. Desiraju, in: Crystal Engineering: The Design of Organic SolidsMaterials Science Monographs, vol. 54, Elsevier Press, 1989.
[11] See for example A.D. Bod, J. Griffiths, J.M. Rawson, J. Hulliger, Chem. Commun. (2001) 2488, and refs therein. See also [10] and references therein.
[12] T. Chivers, K. McGregor, M. Parvez, I. Vargas-Baca, T. Ziegler, Can. J. Chem. (1995) 1380.
[13] A.J. Banister, N. Bricklebank, I. Lavender, J.M. Rawson, C.I. Gregory, B.K. Tanner, W. Clegg, M.R.J. Elsegood, F. Palacio, Angew. Chem., Int. Ed. Engl. 35 (1996) 2533.
[14] E.G. Awere, N. Burford, C. Mailer, J. Passmore, M.J. Schriver, P.S. White, A.J. Banister, M. Oberhammer, L.H. Sutcliffe, J. Chem. Soc., Chem. Commun. (1987) 66.
[15] A. Alberola, R.J. Collis, S.M. Humphrey, R.J. Less, J.M. Rawson, Inorg. Chem. 45 (2006) 1903.
[16] A. Alberola, R.J.Collis, R.J. Less, J.M. Rawson, J. Organomet. Chem, this issue, doi:10.1016/j.jorganchem.2006.11.048.
[17] D. Sellmann, K.P. Peters, R.M. Molina, F.W. Heinemann, Eur. J. Inorg. Chem. 5 (2003) 903.
[18] S.M. Mattar, Chem. Phys. Lett. 300 (1999) 542;
Y.-L. Chung, S.A. Fairhurst, D.G. Gillies, G. Kraft, A.M.L. Krebber, K.F. Preston, L.H. Sutcliffe, G. Ẅolmershauser, Magn. Reson. Chem. 30 (1992) 774.

[19] S.C. Nyburg, C.H. Faerman, Acta Crystallogr Sect. B 41 (1985) 274.
[20] R. Taylor, O. Kennard, J. Am. Chem. Soc. 104 (1982) 5063;
D.S. Reddy, B.S. Goud, K. Panneerselvan, J. Chem. Soc., Chem. Commun. (1993) 663;
N. Ziao, J. Graton, C. Laurence, J.Y. Le Questel, Acta Crystallogr., Sect. B 57 (2001) 850.
[21] R.B. Hammond, M.J. Jones, S.A. Murphy, K.J. Roberts, E.D.L. Smith, H. Klapper, H. Kutzke, R. Docherty, J. Cherryman, R.J. Roberts, P.G. Fagan, Mol. Crys. Liq. Crys. 356 (2001) 389.
[22] See for example: A.M.T. Bell, J.N.B. Smith, J.P. Attfield, J.M. Rawson, K. Shankland, W.I.F. David, New J. Chem. (1999) 565, We have also successfully used XRPD to solve structures of 1 in high and low temperature phases and β-p-NCC_6F_4 CNSSN (J.M. Rawson, A.D. Bond, J. Burley et al., unpubl. work).
[23] A. Alberola, J.M. Rawson, A.L. Whalley, J.Mater.Chem 16 (2006) 2560.
[24] A small number of paramagnetic defect sites would be expected to give rise to a Curie tail (a steady increase in χ upon cooling). The discontinuity in χ on both heating and cooling is clear evidence of a reversible phase transition.
[25] J. van den Brink, New J. Phys. 6 (2004) 201.
[26] PC Spartan Pro. Wavefunction Inc., 18401 Von Karman Avenue, Suite 370, Irvine, CA 92612, USA. Available from: <http://wavefunction.com/>.
[27] A.D. Becke, Phys. Rev. A 38 (1988) 3089;
J.P. Perdew, Phys. Rev. B. 33 (1986) 8822.
[28] J.M. Nedelec, L.L. Hench, J. Non-cryst. Solids (2000) 106;
R.J. Meier, E. Koglin, Macromol., Theory Sim. 13 (2004) 133;
E. Lewars, Can. J. Chem. 78 (2000) 297.